PCCP
Physical Chemistry Chemical Physics

Accepted Manuscript

This article can be cited before page numbers have been issued, to do this please use: M. A. Salvadó, P. Pertierra and J. M. Recio, *Phys. Chem. Chem. Phys.*, 2022, DOI: 10.1039/D2CP04209F.

ROYAL SOCIETY OF CHEMISTRY

rsc.li/pccp

View Article Online
DOI: 10.1039/D2CP04209F

PCCP

ARTICLE TYPE

Cite this: DOI: 00.0000/xxxxxxxxxx

A Mechanism for Aragonite to Post-aragonite Transition in MCO_3 (M = Ca, Sr and Ba) Carbonates: Evidence of a hidden metastable polymorph

Miguel A. Salvadó*, Pilar Pertierra and J. Manuel Recio

Received Date
Accepted Date

DOI: 00.0000/xxxxxxxxxx

To advance in the understanding of the Earth's carbon cycle, it is necessary to determine thermodynamic boundaries and kinetic barriers associated with the pressure-induced polymorphic sequence of alkaline-earth carbonates. Following a symmetry-based strategy within the martensitic approximation, we propose a two-step mechanism mediated by a hexagonal $P6_3/mmc$ structure for the aragonite to post-aragonite transformation in the MCO_3 (M = Ca, Sr, Ba) crystal family. The calculated transition pressures and activation energies, from $\sim$ 7 to 42 GPa and $\sim$ 0.3 to 0.6 eV, respectively, are low enough to allow this transformation to occur under mantle conditions. Our analysis reveals that the intermediate hexagonal structure is the early one proposed by Holl *et al.*, *Phys. Chem. Miner.*, 2000, **27**, 467-473 for high pressure $BaCO_3$, and later considered as metastable. Phonon calculations inform that this $P6_3/mmc$ structure is in fact unstable at zero pressure. Remarkably, our molecular dynamics calculations showed that this instability smoothly leads to a dynamically stable $P6_3mc$ structure, which we confirm is actually the phase observed by Holl *et al.* This finding allows us to reconcile previous controversial data and contributes to clarifying the role of carbonates in the Earth's interior.

1 Introduction

Carbonates, and specially $CaCO_3$, are minerals involved at least in three-fold relevant implications of Earth's carbon cycle: (i) global climate, (ii) carbon energetic reservoirs, and (iii) origin of life.[1–5] The presence of carbonates at different depths of Earth's interior depends on a variety of factors such as subduction processes, density and miscibility, chemical decomposition and reduction, or pressure-induced phase transitions. The thermodynamics and kinetics of carbonate polymorphic sequences are two fundamental aspects in many of these phenomena that deserve further investigation to quantitatively determine phase stability pressure regions and temperatures required to observe the transitions. In particular, the proposal of transition paths connecting high-pressure carbonate polymorphs is still a pending issue that needs to be addressed to complement the thermodynamic view.

Calcite is the thermodynamically stable phase of $CaCO_3$ under room conditions. At pressures as low as 3 GPa, it transforms to the so-called aragonite phase with an orthorhombic *Pnma* space group.[6] Aragonite-type structure is already the stable phase at room conditions of $SrCO_3$ (strontianite) and $BaCO_3$ (witherite).[7] The phases occurring at higher pressures in the three compounds have been the center of a number of experimental and computational investigations in the last two decades that provide a wealth of information and also leave some questions open. Holl *et al.*[7] found a displacive, first-order transformation from witherite to the trigonal space group $P\bar{3}1c$ ($BaCO_3$-II). In $CaCO_3$, Santillán and Williams[8] found experimentally a transition from aragonite to a new phase at 50 GPa and proposed a trigonal structure related to that found previously for $BaCO_3$. The experiments of Ono *et al.*[9–11] suggested orthorhombic structures for the high pressure phases of $CaCO_3$, $SrCO_3$ and $BaCO_3$, and proposed, based on DFT calculations, that the trigonal $BaCO_3$ structure were metastable.[12] Subsequently, other experimental[13–15] and theoretical[16–18] studies seem to confirm a so-called "post-aragonite" phase of *Pmmn* symmetry as the high pressure phase in $CaCO_3$, $SrCO_3$ and $BaCO_3$ with some of these studies pointing to the trigonal phase as metastable in the case of $BaCO_3$.[13,19,20] Other computational investigations have found, among others, other possible high pressure monoclinic ($P2_1/c$) forms for $CaCO_3$: *monolow1*[21,22] and *monolow2*[23], and also found some experimental evidences for *monolow1*.[23–25] Clearly, all these results evidence the existence of kinetic barriers preventing the emergence of the true thermodynamic stable phase and opening the possibility of observing metastable structures in the alkaline-earth

MALTA-Consolider Team and Departamento de Química Física y Analítica, Universidad de Oviedo. E-33006 Oviedo, Spain
*Corresponding author;e-mail:mass@uniovi.es

View Article Online
DOI: 10.1039/D2CP04209F

pressure-induce polymorphic sequence of the carbonate family.

When kinetic aspects are at play, the study of paths connecting minima on the potential energy surface (PES) of compounds becomes necessary.[26,27] These paths traverse through saddle points that correspond to unstable structures. The status of a structure as stable, metastable, or unstable is not fixed but depends on temperature and pressure conditions. This is of particular relevance in the context of the alkaline-earth carbonate crystal family, where the sequence of observed phases shows similarities but also absences and peculiarities along this series. In spite of not being found, the absent structures can play a role in the PES of others members of the crystal family in the form of local minima (metastable phases) or saddle points (unstable structures). As these saddle points connect minima representing either stable or metastable structures, their characterization is key in the proposal of reliable transition mechanisms for solid-solid transformations. Saddle points also provide information about these kinetic aspects that are less commonly studied, and are by no doubt more helpful to adequately explain the experimentally observed phases than the pure thermodynamic data. For example, information about the barrier heights involved in reconstructive phase transitions can be directly translated, using an adequate model, to temperature values at which the available thermal energy of the compound is high enough to allow the transition to occur.[28]

Although several automatic procedures have been recently developed to explore crystal PESs and evaluate minimal energy paths (see for example Refs. 29–31), we believe that a symmetry analysis of group-subgroup relationships applied to carbonate structures is still indispensable to envisage chemically founded transition pathways. This approach is especially necessary if many degrees of freedom are present as in the polymorphic sequence of carbonates, where multi-step mechanisms are expected along the transformations. The outcome of this symmetry-based strategy also provides useful results for the more realistic (and computationally more expensive) nucleation and growth models.[32]

To the best of our knowledge, only Smith *et al.* undertook the study of the pressure-induced polymorphism in carbonates under a mechanistic perspective.[23] They evaluated possible pathways between aragonite and *monolow1* structures using the generalized solid-state nudged elastic band (G-SSNEB) method[33] and found a pressure-dependent intricate path with many intermediate minima and maxima, and with an enthalpy barrier around 0.7-0.8 eV/formula unit. In the same paper, they state that they "attempted to define similar pathways from both *Pnma* and $P2_1/c$-l [*monolow1*] to *Pmmn* using 2 unit cells, however in each case we were unable to obtain a satisfactorily converged pathway". According to their results, they speculate that in $CaCO_3$ "these transitions may require temperatures that are beyond those estimated to be in the mantle at 50-80 GPa".

In our study, a symmetry-based computational strategy is applied to the characterization of atomic trajectories and enthalpy profiles across the aragonite-post aragonite transformation in the MCO_3 (M = Ca, Sr and Ba) crystal family. Following this strategy, a general two-step transition path has been disclosed for the three carbonates. Our first-principles calculations provide energy barriers, unit cell distortions, atomic displacements, and changes in the coordination of the carbonate atomic constituents associated with the transition. One of the most relevant findings of our study is the identification of a metastable hexagonal structure easily derived from the unstable intermediate connecting the two steps of the mechanism. This result is specifically discussed in our manuscript in relation to a controversial polymorph observed in high-pressure experiments carried out on $BaCO_3$. Pressure and temperature conditions evaluated for the transition in the three carbonates are also analyzed with regard to the possibility of finding them in the Earth's interior.

2 Methodology

2.1 Computational details

Static total energy calculations of a number of MCO_3 (M = Ca, Sr and Ba) structures were carried out within the DFT framework using the VASP code[34] and the projector augmented wave (PAW) method[35] in a volume grid that covers compression and expansion regions large enough to examine the equilibrium structures and enthalpies at the pressures that we discuss in the mansucript. We used the Perdew-Burke-Ernzerhof (PBE) exchange-correlation functional[36]. The valence configurations $2s^2 2p^2$, $2s^2 2p^4$ and $(n-1)s^2(n-1)p^6 ns^2$ were used for the carbon, oxygen and metallic atoms, respectively. The Brillouin zone was sampled using Γ-centered Monkhorst-Pack meshes[37] where the numbers of subdivisions along each reciprocal lattice vector $\vec{b}_i$ were given by $N_i = \max(1, 15 \times |\vec{b}_i| + 0.5)$. An energy cutoff of 520 eV was used for the plane waves and FFT grids were chosen to include all *G*-vectors 1.5 times larger than those included in the basis set. Self-consistent iterations were performed until convergence on total energies and forces of 10^{-6} eV and 10^{-5} eV Å^{-1}, respectively, were achieved. Test calculations showed that energy cutoff and k-point grids were enough to give energy differences converged below 0.001 eV/atom. Molecular dynamics simulations were also performed with VASP under a canonical NVT ensemble using a Nosé-Hoover thermostat with a time step of 0.7 fs and a Nosé-mass corresponding to a period of 40 time steps. G-SSNEB calculations were done using VASP and the VTST Tools[33]. Phonon dispersion bands were calculated with the `Phonopy` package[38] from DFPT VASP calculations. Equation of state parameters and static transition pressures were obtained using numerical and analytical fittings to the energy-volume data as implemented in the `Gibbs2` code[39]. The symmetry of the structures was analyzed using FINDSYM software[40,41]. Crystal structure plots were made with VESTA[42]. Visualizations of molecular dynamics simulations were done with OVITO[43].

2.2 Crystal Description and Martensitic Approach

In order to describe the structure of carbonates, it is useful to begin considering the underlying net under a quasi-binary representation in the Blatov's description[44]. In this way $CaCO_3$ is a network of the type ML where the structural unit CO_3^{2-} has been contracted to L. The aragonite structure of $CaCO_3$, $BaCO_3$, and $SrCO_3$ have a distorted NiAs net (*Pnma* space group) with an M-L

View Article Online
DOI: 10.1039/D2CP04209F

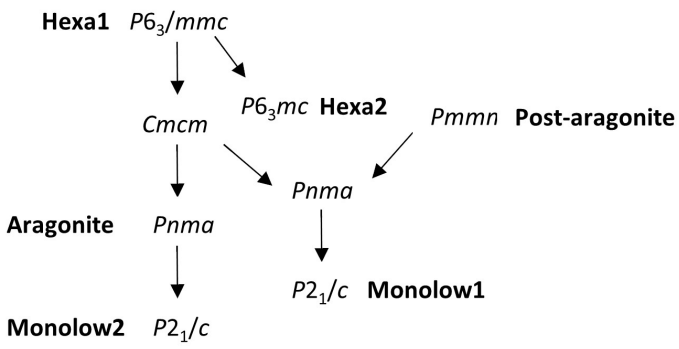

Fig. 1 Group-subgroup relations.

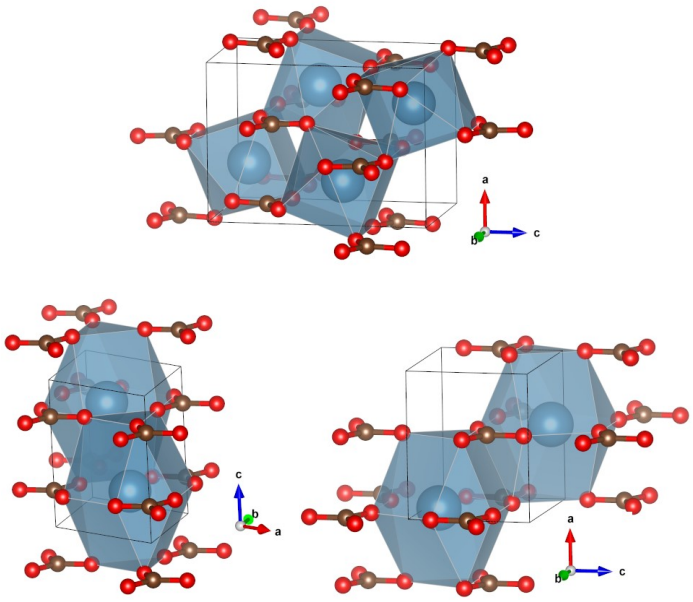

Fig. 2 Polyhedral view of the conventional unit cells of aragonite (top), hexagonal (bottom left), and post-aragonite (bottom right) structures. The alkaline-earth metal is located inside the corresponding blue polyhedra, whereas planar CO_3 units are identified with carbon atoms in brown and oxygen atoms in red.

coordination 6, and they are isostructural with α-KNO_3 (KNO_3-II)[45]. The symbol T^{33} is used by Blatov to denote that of the six carbonates, there are three monodentate (first superscript) and three bidentate (second superscript) which gives 9 as the total oxygen coordination around Ca. The space group of aragonite, *Pnma* and the spacegroup of the ordered NiAs net, $P6_3/mmc$ are related by a group-maximal subgroup chain through the intermediate space group, *Cmcm* as is shown on the left of Figure 1.

Post-aragonite $CaCO_3$ phase (or hp-$CaCO_3$)[46] posses a distorted CsCl net where the Ca atom is eight coordinated (T^{44}) (*Pmmn* space group) and it is isostructural with the high pressure phases of $RbNO_3$, $CsNO_3$[47] and with NH_4NO_3-IV[48]. The (T^{44}) symbol means that each calcium atom is coordinated to 12 oxygen atoms. In the Figure 1 a relationship between the post-aragonite space group and aragonite-hexagonal chain is highlighted. The connection path uses a common *Pnma* subgroup of the *Cmcm* and *Pmmn*, not to be confused with the aragonite *Pnma*.

Although they will be not included in our later discussion, it is interesting to point out that *monolow1* and *monolow2* phases can be related to the post-aragonite and aragonite structures, respectively, and they have been included in Figure 1 for completeness.

Here, we propose a mechanism for aragonite to post-aragonite transformation through an intermediate hexagonal $P6_3/mmc$ structure. In the first stretch, aragonite evolves to the hexagonal structure (path1), whereas in the second part the post-aragonite phase is reached starting from the hexagonal structure (path2). Aragonite belongs to the *Pnma* space group. Its conventional unit cell contains four formula units: 4 Ca, 4 C and 12 O atoms with Ca and C at $4c(x,1/4,z)$ positions and oxygen atoms at $4c(x,1/4,z)$ and general $8d(x,y,z)$ positions. Post-aragonite belongs to the *Pmmn* space group. Its conventional unit cell contains two formula units: 2 Ca, 2 C and 6 O atoms with Ca at $2c(0,1/2,z)$, C at $2a(0,0,z)$, and oxygen atoms at $4e(0,y,z)$ and $2a(0,0,z)$. The intermediate hexagonal structure belongs to the $P6_3/mmc$ space group. Its conventional unit cell contains two formula units: 2 Ca, 2 C and 6 O atoms with Ca at $2d(1/3,2/3,z)$, C at $2b(0,0,1/4)$, and O at $6h(x,2x,1/4)$. A polyhedral view of the three unit cells is presented in Fig. 2.

In path1 (aragonite to hexagonal), we use the conventional unit cell of aragonite to describe the mechanism because the aragonite space group (*Pnma*) is a subgroup of $P6_3/mmc$. It is really a maximal subgroup of *Cmcm*, a maximal subgroup of $P6_3/mmc$ (see Figure 1). The orthorhombic cell is related to the conventional hexagonal by the transformation $-\mathbf{c}$, $-\mathbf{a}$, $\mathbf{a}+2\mathbf{b}$. In this description, the hexagonal structure has the atoms in the same Wyckoff positions as the aragonite structure. The x coordinate of carbon, x_C, is selected as the transformation coordinate along this path1 (see below). In path2 (hexagonal to post-aragonite), a unit cell in a common subgroup *Pnma* (involving again the subgroup *Cmcm*) with four formula units is chosen to describe the mechanism. We note that although being the same space group type and being subgroups of the same structure, this *Pnma* structure is different from the aragonite one. This cell is related to the hexagonal one by the transformation $-\mathbf{a}-2\mathbf{b}$, $-\mathbf{c}$, $\mathbf{a}$; and to the post-aragonite by the transformation $2\mathbf{c}$, $\mathbf{a}$, $\mathbf{b}$; and contains 4 Ca, 4 C and 12 O atoms with all atoms at $4c(x,1/4,z)$ positions. For

View Article Online
DOI: 10.1039/D2CP04209F

this path2, the transition coordinate is the z coordinate of C, z_C.

To determine the transition path at a certain pressure, we start with the equilibrium structure of aragonite at that pressure. At each step of the first path, we update the x_C value, fixing it at each step and relaxing the rest of the atomic and cell degrees of freedom while maintaining the orthorhombic symmetry and the pressure constant at its equilibrium value. When the hexagonal structure is reached, cell and coordinates are transformed to the *Pnma* second subgroup, the reaction coordinate is changed to z_C and this value is updated following a similar process.

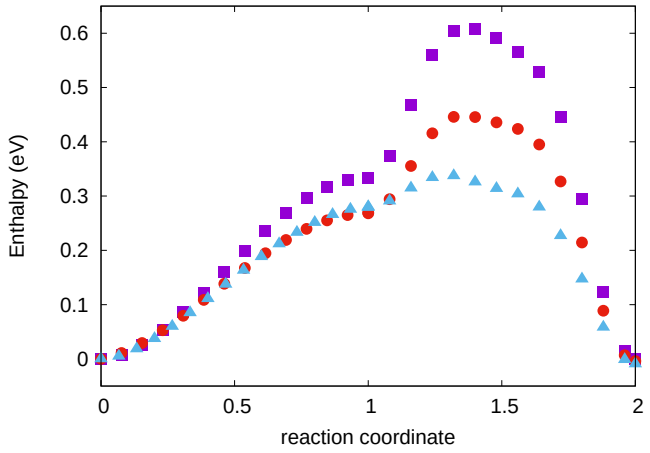

Fig. 3 Calculated enthalpy profiles of Ca (purple squares), Sr (red circles), and Ba (blue triangles) carbonates aragonite to post-aragonite transitions according to the proposed two-path mechanism.

3 Results and Discussion

3.1 Aragonite to Post-aragonite Transition Path

Calculated energy-volume (E-V) curves for the aragonite, post-aragonite and hexagonal phases for the three carbonates are collected in Fig. S1, and the corresponding EOS parameters are collected in Table S1. The predicted static transition pressures to post-aragonite evaluated from these curves are 41.6, 17.4, and 7.3 GPa for Ca, Sr, and Ba carbonates, respectively. In Figure 3, the enthalpy profile along path1 plus path2 is shown for the three carbonates at their respective transition pressures. Values of the two transition coordinates, x_C and z_C, were normalized to change from 0 to 1 (path1) and from 1 to 2 (path2), respectively. For $CaCO_3$ the barrier is around 0.6 eV/formula unit, for $SrCO_3$ 0.45 eV, and for $BaCO_3$ 0.3 eV.

The path1 corresponds to a displacement of carbonate groups along the x axis, whereas in the path2 the carbonate groups are displaced along the direction of the z axis (the original y axis). The whole transition path is formally equivalent for the three carbonates. For the sake of brevity, quantitative description is given only for $CaCO_3$. For path1 (path2), at each step of the transformation coordinate, atomic displacements (relative to the atomic positions in the cell at the previous step) were calculated to be less than 0.051 (0.129) Å. The total Ca, C and O (two different O atoms for path1 and three different O atoms for path2) displacements relative to the initial cell, were 0.035 (1.18), 0.63 (1.16) and 0.58, 0.61 (1.16, 1.18, 1.14) Å, respectively. For the final cell, hexagonal and post-aragonite respectively, the degree of lattice distortion,[49] the so-called spontaneous strain S defined as the square root of the sum of the squared eigenvalues of the strain tensor divided by 3, referred to as the initial cell was $S =$ 0.0331 (0.0158), whereas the lattice distortions at each step were less than 0.005 (0.005).

In Figure 4 selected crystal structures along the path are shown. The path1 begins with the aragonite structure (x_C = 0.88) and ends with the $P6_3/mmc$ structure that we name *hexa1* from now on (x_C = 0.75). The planes of carbonate groups move perpendicularly until they match with the planes of calcium atoms. In terms of oxygen coordination around calcium atoms, the structure changes from 9 to 12, corresponding to an increase in the number of carbonate groups around each calcium from 6 to 9. In the path2, the starting *hexa1* structure (now labeled with the new transition coordinate z_C = 0.50) is now represented as seen from above the carbonate and calcium planes, making visible the hexagonal symmetry. Carbonate groups are now moving within the above-mentioned planes with alternate rows moving in opposite directions, and calcium atoms are following some of the carbonate ions in this displacement in order to keep a large part of Ca-O interactions. Along this step, the oxygen coordination does not change (12), although the number of carbonate groups around the calcium atoms reduces from 9 to 8.

Relevant changes in Ca-C and Ca-O distances are shown in Fig. 5 and Fig. 6, for path1 and path2, respectively. In the aragonite, the six carbonate groups can be divided into two coordination spheres: one of them was formed by three carbonates with Ca-C distances between 2.6 and 2.8 Å (C1 and two equivalent C2 carbon atoms) and another one was formed by three carbonates between 3 and 3.2 Å (two C3 and C4). The carbonates of the first sphere are bidentate, that is, joined by two oxygen atoms to the same calcium atom, whereas the carbonates of the second sphere are monodentate, that is, joined only through one oxygen atom to that calcium atom. This is symbolized in Blatov notation as T^{33} coordination and makes a total of nine oxygen atoms around each calcium atom. These nine oxygen atoms are at distances between 2.2 to 2.4 Å from calcium.

In the path1 on the way to the hexagonal structure, the three carbonates of the second shell are moving away to 3.5 Å whereas three additional carbonates (C5 and two C6) approach this distance, accounting for a total of six monodentate carbonates. Twelve oxygen atoms surround each calcium in two shells, six of them at about 2.3 Å (O2, O3, O5), corresponding to the three bidentate carbonates, and the other six at about 2.6 Å (O1, O4, O6, O7), corresponding to the six monodentate carbonates (T^{63}). All the atoms in this path1 are well identified in the central panel of Fig. 5.

In the path2, two monodentate carbonates of the second shell are moving away to a distance greater than 4 Å (two C4 atoms and two O8 atoms) whereas one distant monodentate carbonate is approaching (C7 through O11). Simultaneously, two already coordinated carbonate changes from monodentate to bidentate (C5 increase their link to metal through O10) and another one from bidentate to monodentate (C3 lose its metal link through O5) thus preserving the number of 12 coordinating oxygen atoms

View Article Online
DOI: 10.1039/D2CP04209F

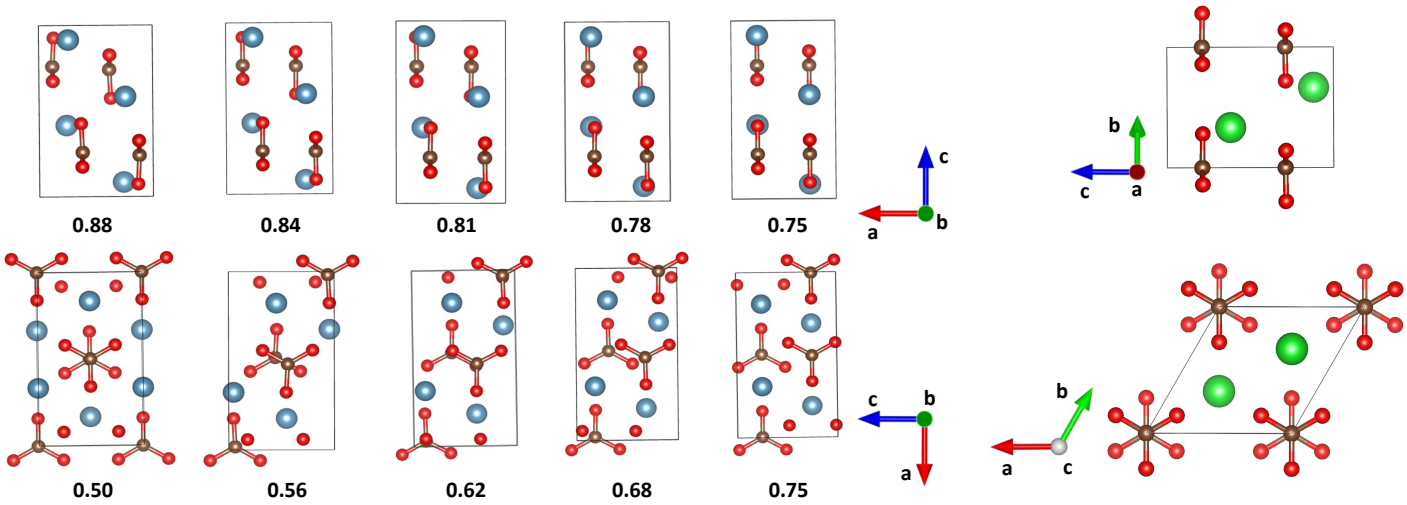

Fig. 4 Left: Snapshots of $CaCO_3$ crystal structures along path1 (top) and path2 (bottom). Below each plot, the value of the parameter used as the transition coordinate is shown. Right: Two views of $BaCO_3$ *hexa2* structure along *a* axis (top) and along *c* axis (bottom). Ca, Ba, C, and O atoms are represented by blue, green, brown, and red spheres, respectively.

and building the post-aragonite structure (T^{44}) where there are a total of eight carbonate groups around each calcium distributed in two shells, the first one (four bidentate groups) with distances between 2.6 to 2.8 Å, the second one (four monodentate groups) with distances between 3.2 to 3.5 Å. Equivalently to path1, the central panel of Fig. 6 contains the symbols associated with the atomic positions of carbon and oxygen along this path2.

Changes in cell volume and cell parameters across the whole transition path are shown in Fig. 7. The second path captures an increase in the cell volume in the middle of this step with a final net reduction similar to the one found after the first path. At the value of the transition coordinate with the highest cell volume, Ca shows the most crowded surrounding. C and O atoms leaving and approaching Ca display values around 3.1-3.3 Åleading to a second coordination sphere of Ca with more neighbors than at another point of the transition path. This constrained environment is released by increasing the volume of the unit cell. All these structural parameters inform a smooth evolution of the atomic trajectories and cell shape across the two transition steps with more pronounced changes in path2.

The energy barrier we have found for the transition from the aragonite to the post-aragonite structure in $CaCO_3$ is of the same order that the one found by Smith *et al.* [23] in their proposed mechanism from aragonite to *monolow1*, although our calculated value is slightly lower by 0.1-0.2 eV. Notice that the highest enthalpy point is reached in path2 as expected for the greater atomic displacements obtained in this stretch. This value is almost reduced by two (around 0.3 eV in $CaCO_3$) to reach the hexagonal structure at the end of path1. Using a simple Debye model implemented in the GIBBS2 program [39], we evaluate the available vibrational energy of the three carbonates at different temperatures in order to estimate the temperature at which the energy barrier found for the aragonite-post-aragonite transition can be overcome. The estimation is obtained considering only 2 atoms per formula unit since "CO_3" acts as a unique entity (the internal vibrational modes of the carbonate unit do not play a role in the transition mechanism). The calculated values for $CaCO_3$, $SrCO_3$, and $BaCO_3$ at their respective equilibrium transition pressures are 1150, 900, and 600 K, respectively. The temperature for $CaCO_3$ (1150 K), along with the transition pressure (41.6 GPa), and the density of the high-pressure phase ($\sim$ 4.1 g/cm^3) make it not possible to find the post-aragonite phase of the calcium carbonate at the upper mantle, but at the top of the lower mantle, at depths beyond the transition zone and around 1000 km. We have seen that the intermediate hexagonal structure is reached requiring a lower energy barrier and then lower vibrational energy and a lower temperature is needed. Its density is slightly lower ($\sim$4.0 g/cm^3) than aragonite, although a pressure above 40 GPa is also required since it appears along the aragonite to post-aragonite transition path.

In order to check whether the proposed mechanism corresponds to a minimum energy path, G-SSNEB calculations were carried out using the knowledge obtained in our previous analysis and splitting the path into the two steps described above. In Fig. S2, the corresponding enthalpy profile for $CaCO_3$ is shown. The obtained path is exactly the same as the one we had proposed, differing only in the definition of the transition coordinate.

3.2 A metastable hexagonal structure

The *hexa1* structure constitutes an intermediate structure in the path described above that deserves further examination. In the light of Fig. 3, it is not a metastable structure, at least at low temperatures, for any of the three carbonates at the pressures used in the respective paths. We carried out a NVT molecular dynamics study of $BaCO_3$ at 300K, using as the simulation cell the orthorhombic one without symmetry constraints and starting from the hexagonal structure at 0 GPa. The results revealed that the *hexa1* structure transforms easily to another one that was maintained on average along the simulation and when optimized at zero pressure resulted in a hexagonal phase with symmetry $P6_3mc$ (*hexa2* phase). This structure (see Figure 4 right) resembles the aragonite phase as the coordination numbers around Ca

View Article Online
DOI: 10.1039/D2CP04209F

are concerned (6 carbonate groups and 9 oxygen atoms).

Phonon dispersion bands for the *hexa1* and *hexa2* structures are shown in Fig. 8. These phonon dispersion bands show the well-known [18,50] five regions of bands: the four upper are internal carbonate modes (12) related to carbonate group distortions,

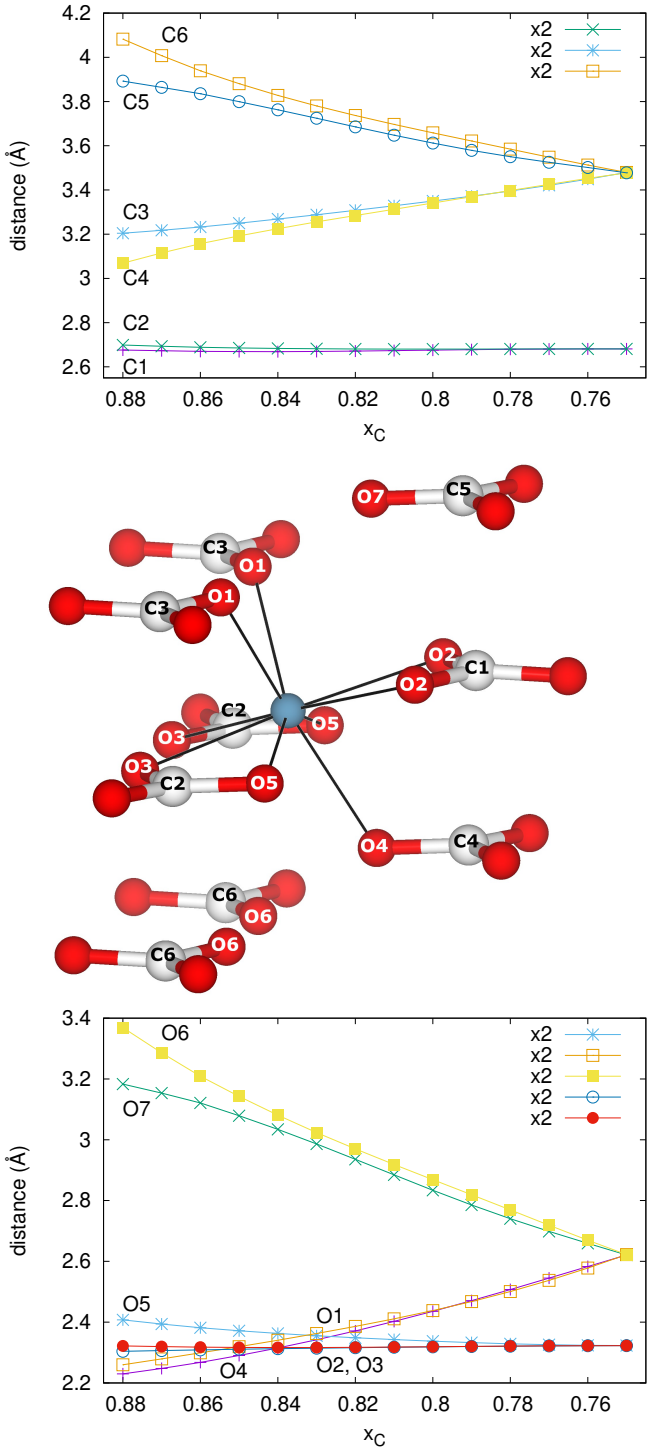

Fig. 5 Change in distances along path1 for Ca-C (top) and Ca-O (bottom) for $CaCO_3$. Distances labeled 'x2' corresponds to two equivalent atom pairs. Relevant carbon (labels C1 to C6) and oxygen (labels O1 to O7) atoms surrounding Ca (in blue) involved in path1 are displayed in the central panel.

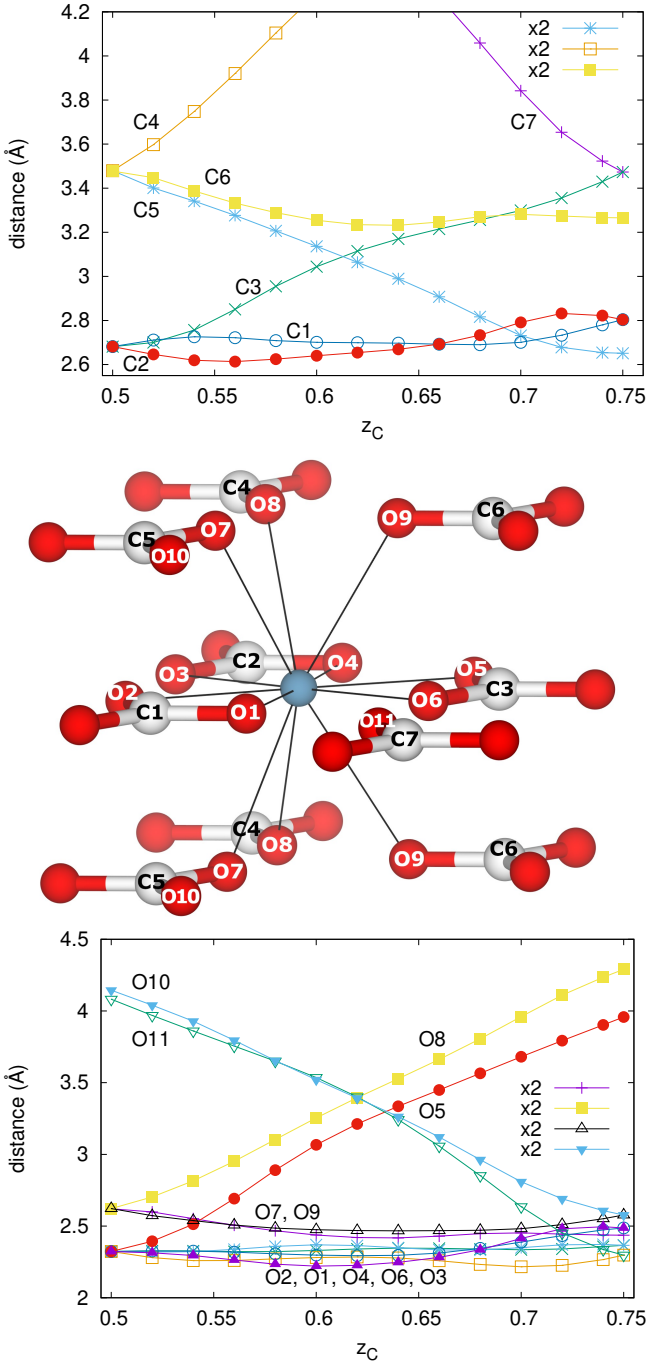

Fig. 6 Change in distances along path2 for Ca-C (top) and Ca-O (bottom) for $CaCO_3$. Distances labeled 'x2' corresponds to two equivalent atom pairs. Relevant carbon (labels C1 to C7) and oxygen (labels O1 to O11) atoms surrounding Ca (in blue) involved in path2 are displayed in the central panel.

and the region under 10 THz corresponds to the 18 modes of 2 Ba translations + 2 rigid CO_3 translations and rotations. For the *hexa1* structure we have imaginary modes along the major part of the first Brillouin zone. At Γ-point, we have only one imaginary mode that corresponds to an A_{2u} symmetry. When the eigenvector corresponding to this mode is calculated and analyzed, it corresponds to an optic mode consisting essentially in a translation of Ba and CO_3 ions along z direction in opposite directions. This is

View Article Online
DOI: 10.1039/D2CP04209F

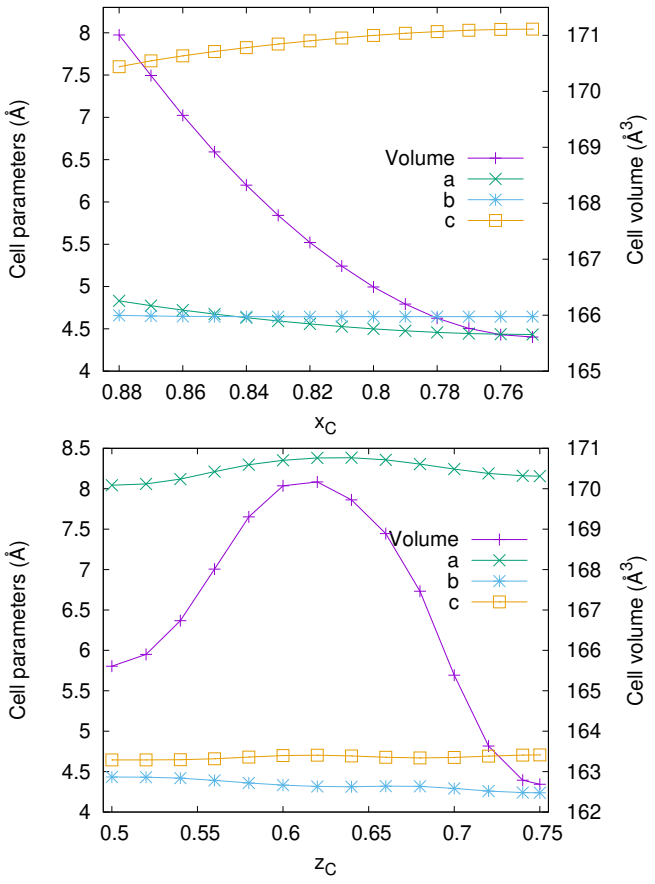

Fig. 7 Change in cell volume and cell parameters along path1 (top) and path2 (bottom) for $CaCO_3$; a, b and c are the lattice parameters of the respective unit cells

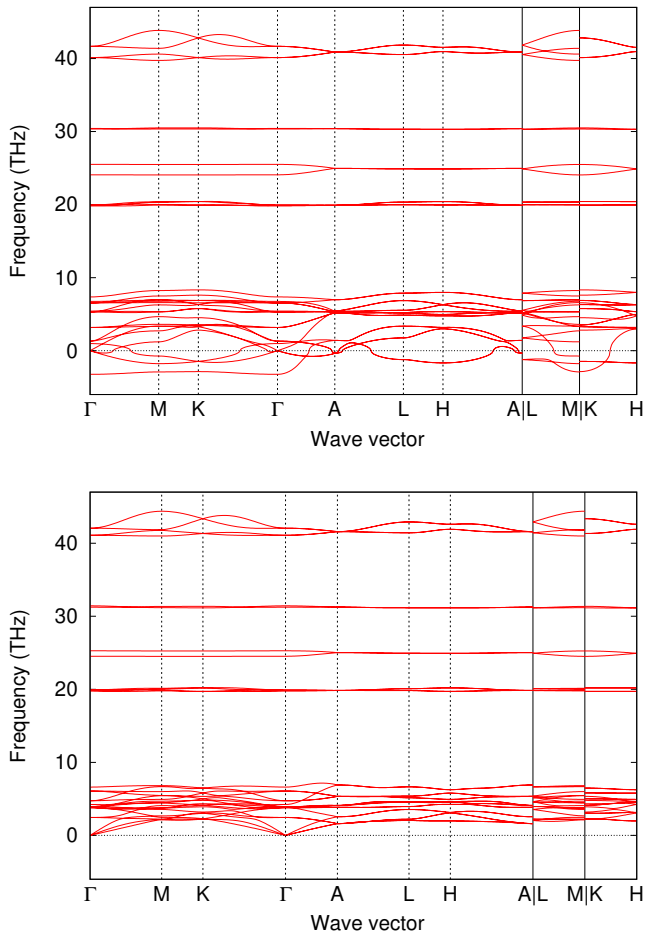

Fig. 8 Phonon dispersion of *hexa1* (top) and *hexa2* (bottom) $BaCO_3$

the kind of displacement that leads to the *hexa2* structure, as we can see in Fig. 4. In the case of *hexa2*, the phonon dispersion bands show the dynamical stability of the structure.

We identify this structure as the hexagonal (previously assigned as trigonal) observed by Holl *et al.*[7] for $BaCO_3$-II. Our calculated cell for *hexa2* at 8.3 GPa is $a = 5.275, c = 5.644$ Å, $V = 136$ Å^3, that is very similar to the reported experimental cell at 7.2 GPa, $a = 5.258, c = 5.64$ Å, $V = 135$ Å^3. Holl et al. described this structure in $P\bar{3}1c$ space group using a small diffraction data set. Using their cell and atom data, our analysis of crystal symmetry[40,41] revealed a higher symmetry, the hexagonal $P6_3/mmc$ space group (minimal supergroup) and it would therefore be identical to *hexa1*. The space group of *hexa2*, $P6_3mc$, is another maximal subgroup of $P6_3/mmc$, possesses the same reflection conditions that $P\bar{3}1c$ and could, then, have been misidentified. The relationship between the space group of *hexa2* and the other phases was also included in the group-subgroup figure (Figure 1). Very recently, the role of another hexagonal polymorph ($P6_322$) as an intermediate in the calcite to aragonite transformation has been analyzed[51]. Interestingly enough, the space group of this phase is another maximal subgroup of the $P6_3/mmc$ parent structure. The difference here relies on a 30º rotation of carbonate groups. Then, a unified view of the relationships between calcite, aragonite, and post-aragonite structures can probably emerge, and it deserves future study.

E-V curves for the *hexa1* and *hexa2* phases are shown in Fig. S1, along with aragonite and post-aragonite. The relative positions of the corresponding enthalpy-pressure curves are shown in Fig. S3. These results indicate that *hexa2* is not the lowest enthalpy structure for any of the three compounds in the pressure range studied, but is close in enthalpy to the aragonite structure, especially in the Sr and Ba carbonates. For Sr, a metastable transition would occur at 70 GPa and for Ba this would occur at 30 GPa. $BaCO_3$ is the only case where the observation of a transition from aragonite to the hexagonal phase has been reported, and the experimental pressure at ambient temperature was 7.2 GPa. Because the transition from aragonite to the post-aragonite phase requires higher activation energy, it is not surprising that compression of aragonite at room temperature could lead to the metastable hexagonal phase. Our predicted transition pressure is considerably higher than the one observed experimentally. An explanation of this difference relies on the fact that due to the relatively low energy barrier associated with carbonate displacements along the *c* axis of the hexagonal structure, one can easily devise a number of structural variations with part of the carbonate ion columns arranged either in *hexa2* or in aragonite form. We have tried one of these possibilities (see Fig. S4) and have obtained a metastable structure with slightly lower energy than

View Article Online
DOI: 10.1039/D2CP04209F

hexa2. It should be also taken into account that a hypothetical disordered structure built under this structural idea would be entropically stabilized.

4 Conclusions

Thanks to a detailed symmetry analysis we were able to provide a consistent mechanism for the transformation from aragonite to post-aragonite, which was confirmed by NEB calculations. This mechanism consists of two steps going through an unstable intermediate hexagonal structure. The first step is not activated, but the second goes through an enthalpy maximum that determines the energy barrier of the mechanism. The barrier height for the transition in $CaCO_3$ at the thermodynamic transition pressure corresponds to thermal energy compatible with the conditions at the earth's top lower mantle. For the $SrCO_3$ and $BaCO_3$ the barrier heights are lower (in that order).

The hexagonal intermediate structure turns out to be the trigonal one proposed by Holl *et* al.[7] as a high pressure phase of $BaCO_3$ and that more recently has been considered metastable. In fact, this phase can stabilize without cell change going to a maximal subgroup. The importance of this finding is two-fold. First, this structure (or a disordered variant) is a reasonable candidate for the phase that Holl *et al.* observed and labeled as $BaCO_3$-II. Second, it is detected as a hidden structure that could be potentially observed metastable in other carbonates if the conditions are appropriate.

Conflicts of interest

There are no conflicts to declare.

Acknowledgements

Financial support from Spanish National Research Agency (AEI) through projects PGC2018-094814-B-C2 and RED2018-102612-T, and from Principado de Asturias (FICYT) and FEDER under project AYUD/2021/51036 are gratefully acknowledged. We thank MALTA-Consolider supercomputing center for computer facilities.

Notes and references

1 R. Hazen, R. Hemley and A. Mangum, *EOS Trans. Am. Geophys. Union*, 2012, **93**, 17–18.
2 R. Hazen and C. Schiffries, *Rev. Mineral. Geochem.*, 2013, **75**, 1–6.
3 M. Merlini, S. Milani and J. Maurice, in *Structures and Crystal Chemistry of Carbonate at Earth's Mantle Conditions*, Amer. Geophys. Union (AGU), 2020, ch. 9, pp. 87–95.
4 R. Chuliá-Jordán, D. Santamaria-Perez, J. Ruiz-Fuertes, A. Otero-de-la Roza and C. Popescu, *ACS Earth Space Chem.*, 2021, **5**, 1130–1139.
5 J. Gao, X. Wu, X. Yuan and W. Su, *Frontiers in Earth Science*, 2022, **10**,.
6 B. Dickens and J. S. Bowen, *J. Res. Natl. Bur. Stand. Phys. Chem. A*, 1971, 27–32.
7 C. M. Holl, J. R. Smyth, H. M. S. Laustsen, S. D. Jacobsen and R. T. Downs, *Phys. Chem. Miner.*, 2000, **27**, 467–473.
8 J. Santillán and Q. Williams, *Amer. Mineral.*, 2004, **89**, 1348–1352.
9 S. Ono, T. Kikegawa, Y. Ohishi and J. Tsuchiya, *Amer. Mineral.*, 2005, **90**, 667–671.
10 S. Ono, M. Shirasaka, T. Kikegawa and Y. Ohishi, *Phys. Chem. Miner.*, 2005, **32**, 8–12.
11 S. Ono, *Phys. Chem. Miner.*, 2007, **34**, 215–221.
12 S. Ono, J. P. Brodholt and G. D. Price, *Mineral. Mag.*, 2008, **72**, 659–665.
13 J. Townsend, Y.-Y. Chang, X. Lou, M. Merino, S. Kirklin, J. Doak, A. Issa, C. Wolverton, S. Tkachev, P. Dera and S. Jacobsen, *Phys. Chem. Miner.*, 2013, **40**, 447–453.
14 M. Wang, Q. Liu, S. Nie, B. Li, Y. Wu, J. Gao, X. Wei and X. Wu, *Phys. Chem. Miner.*, 2015, **42**, 517–527.
15 N. Biedermann, E. Bykova, W. Morgenroth, I. Efthimiopoulos, J. Mueller, G. Spiekermann, K. Glazyrin, A. Pakhomova, K. Appel and M. Wilke, *Eur. J. Mineral.*, 2020, **32**, 575–586.
16 W. Sekkal, N. Taleb, A. Zaoui and I. Shahrour, *Amer. Mineral.*, 2008, **93**, 1608–1612.
17 S. Arapan and R. Ahuja, *Phys. Rev. B*, 2010, **82**, 184115 [1–8].
18 M. Ukita, K. Toyoura, A. Nakamura and K. Matsunaga, *J. Appl. Phys.*, 2016, **120**, 142118 [1–8].
19 A. Zaoui and I. Shahrour, *Philos. Mag. Lett.*, 2010, **90**, 689–697.
20 J. Chaney, J. Santillán, E. Knittle and Q. Williams, *Phys. Chem. Miner.*, 2015, **42**, 83–93.
21 C. J. Pickard and R. J. Needs, *Phys. Rev. B*, 2015, **91**, 104101 [1–7].
22 S. S. Santos, M. L. Marcondes, J. F. Justo and L. V. Assali, *Phys. Earth Planet. Inter.*, 2020, **299**, 106327 [1–9].
23 D. Smith, K. V. Lawler, M. Martinez-Canales, A. W. Daykin, Z. Fussell, G. A. Smith, C. Childs, J. S. Smith, C. J. Pickard and A. Salamat, *Phys. Rev. Mater.*, 2018, **2**, 013605 [1–11].
24 P. N. Gavryushkin, N. S. Martirosyan, T. M. Inerbaev, Z. I. Popov, S. V. Rashchenko, A. Y. Likhacheva, S. S. Lobanov, A. F. Goncharov, V. B. Prakapenka and K. D., *Cryst. Growth Des.*, 2017, **17**, 6291–6296.
25 L. Bayarjargal, C.-J. Fruhner, N. Schrodt and B. Winkler, *Phys. Earth Planet. Inter.*, 2018, **281**, 31–45.
26 G. Henkelman, *Annu. Rev. Mater. Res.*, 2017, **47**, 199–216.
27 N. Allan, S. Conejeros, J. Hart and C. Mohn, *Theor. Chem. Acc.*, 2021, **140**, 151 [1–16].
28 J. M. Recio, J. M. Menéndez and A. O. De la Roza, *An introduction to high-pressure science and technology*, CRC Press, 2016.
29 A. Oganov, A. Lyakhov and M. Valle, *Acc. Chem. Res.*, 2011, **44**, 227–37.
30 K. Yin, P. Gao, X. Shao, B. Gao, H. Liu, J. Lv, J. S. Tse, Y. Wang and Y. Ma, *npj Comput. Mater.*, 2020, **6**, 16 [1–10].
31 P. A. Santos-Florez, H. Yanxon, B. Kang, Y. Yao and Q. Zhu, *Size-Dependent Nucleation in Crystal Phase Transition from Machine Learning Metadynamics*, 2022, `https://arxiv.org/abs/2205.13631`.
32 M. Badin and R. Martoňák, *Phys. Rev. Lett.*, 2021, **127**,

View Article Online
DOI: 10.1039/D2CP04209F

105701.
33 D. Sheppard, P. Xiao, W. Chemelewski, D. D. Johnson and G. Henkelman, *J. Chem. Phys.*, 2012, **136**, 074103 [1–8].
34 G. Kresse and J. Furthmüller, *Comput. Mater. Sci.*, 1996, **6**, 15–50.
35 P. E. Blöchl, *Phys. Rev. B*, 1994, **50**, 17953–17979.
36 J. P. Perdew, K. Burke and M. Ernzerhof, *Phys. Rev. Lett.*, 1996, **77**, 3865–3868.
37 H. J. Monkhorst and J. D. Pack, *Phys. Rev. B*, 1976, **13**, 5188–5192.
38 A. Togo and I. Tanaka, *Scr. Mater.*, 2015, **108**, 1–5.
39 A. Otero-de-la-Roza, D. Abbasi-Pérez and V. Luaña, *Comput. Phys. Commun.*, 2011, **182**, 2232–2248.
40 H. T. Stokes and D. M. Hatch, *J. Appl. Crystallogr.*, 2005, **38**, 237–238.
41 H. T. Stokes, D. M. Hatch and B. J. Campbell, *FINDSYM, ISOTROPY Software Suite, iso.byu.edu*.
42 K. Momma and F. Izumi, *J. Appl. Crystallogr.*, 2008, **41**, 653–658.
43 A. Stukowski, *Model Simul. Mat. Sci. Eng.*, 2010, **18**, 015012 [1–7].
44 V. A. Blatov, in *Crystal Structures of Inorganic Oxoacid Salts Perceived as Cation Arrays: A Periodic-Graph Approach*, ed. A. Vegas, Springer Berlin Heidelberg, Berlin, Heidelberg, 2011, pp. 31–66.
45 D. A. Edwards, *Z. Kristallogr. - Cryst. Mater.*, 1931, **80**, 154–163.
46 A. R. Oganov, C. W. Glass and S. Ono, *Earth Planet. Sci. Lett.*, 2006, **241**, 95–103.
47 M. S. Kalliomäki and V. P. J. Meisalo, *Acta Crystallogr. B*, 1979, **35**, 2829–2835.
48 C. S. Choi, J. E. Mapes and E. Prince, *Acta Crystallogr. B*, 1972, **28**, 1357–1361.
49 C. Capillas, J. M. Perez-Mato and M. I. Aroyo, *J. Phys. Condens. Matter*, 2007, **19**, 275203 [1–16].
50 M. Prencipe, F. Pascale, C. Zicovich-Wilson, V. Saunders, R. Orlando and R. Dovesi, *Phys. Chem. Miner.*, 2004, **31**, 559–564.
51 P. N. Gavryushkin, A. B. Belonoshko, N. Sagatov, D. Sagatova, E. Zhitova, M. G. Krzhizhanovskaya, A. Rečnik, E. V. Alexandrov, I. V. Medrish, Z. I. Popov and K. D. Litasov, *Cryst. Growth Des.*, 2021, **21**, 65–74.